Analysis of Power Electronics-Dominated Hybrid AC/DC Grid for Data-Driven Oscillation Diagnosis

Haoxiang Zong[1], Chen Zhang[1*], Xu Cai[1*] and Marta Molinas[2]
1 Key Laboratory of Control of Power Transmission and Conversion of Ministry of Education, Shanghai Jiao Tong University, Shanghai, China
2 Department of Engineering Cybernetics, Norwegian University of Science and Technology, Trondheim, Norway
*E-mail: haoxiangzong@sjtu.edu.cn

***Abstract*- The high penetration of renewables has imposed great oscillation risks on power grids, especially for the power electronics-dominated hybrid AC/DC grid. Measurement data-driven diagnosis of oscillations regarding where, why and how they happened is crucial to the emergency control. However, before implementing any data-driven diagnosis, a comprehensive analysis of the system oscillation is required. In this paper, a frequency-domain network model of the hybrid AC/DC grid is established, considering both ac- and dc- side dynamics. Based on such model, the frequency-domain modal analysis (FMA) method is introduced to its oscillation assessment, where information like participation factor can be extracted. Finally, the mapping relationship between FMA results and measurement data is identified, laying the ground for data-driven oscillation diagnosis. Case studies are conducted in a typical hybrid AC/DC grid to validate the accuracy of the above analysis.**

Keywords— data-driven; hybrid AC/DC grid; modal analysis; oscillation;

I. INTRODUCTION

Modern power system is undergoing a paradigm shift from the synchronous generators-dominated system to the power electronics-dominated (PED) system [1]. A key driving force behind this scenario is the global need of green energy consumption, where large number of renewable power generations (RPGs) such as large wind farms and solar power plants have been constructed. In this context, power electronics converters are widely deployed in those RPGs serving as their grid interfaces. Therefore, the future power system will exhibit itself as a power electronics-dominated hybrid AC/DC grids [2], [3].

With substantial converters integrated into the system, the dynamic behaviors of conventional power systems are gradually influenced and shaped. Indeed, recent practices [4] in operating such systems have shown that the converters are prone to provoke wideband oscillations [5] (e.g., sub-synchronous oscillations and harmonic oscillations) when connected with the AC grids. Various studies [6], [7] have been conducted in this respect, and a popular example is via the impedance approach [8], from which the fundamental mechanism of those oscillations have been revealed, i.e., the control interactions of converters with the AC grids, particularly those with low short-circuit ratio (SCR).

Aside from the oscillation mechanism, knowledge of how these oscillations will spread in the grid with multiple converters is even more relevant and crucial from the system operation point of view. For the convenience of online monitoring and emergency control [9], it is preferred that the above oscillation information can be extracted from the real-time measurement data, i.e., so-called data-driven diagnosis. However, before carrying out any data-driven diagnosis, a comprehensive oscillation analysis is required in advance. In this regard, the frequency-domain modal analysis (FMA) [10] is usually applied together with the impedance approach for the oscillation analysis of a PED AC grid [11], [12], based on which information on why and where the oscillation occurs can be identified. Despite this success of the FMA method in the PED AC grids, its applicability and effectiveness in the oscillation analysis of a hybrid AC/DC grid have not been discussed. Therefore, this paper will move along in this direction by performing: 1) establish a frequency-domain network model of the hybrid AC/DC grid; 2) implement the FMA-based oscillation analysis of the established network model. After that, FMA results can be compared with measurement data to figure out the mapping relationship between.

II. FREQUENCY-DOMAIN NETWORK MODELLING

A. Building Block of AC/DC Components

A typical power electronics-dominated hybrid AC/DC grid is composed of AC/DC converters and AC/DC passive components. To facilitate the following network modeling, the concept of the building block is introduced to characterize the above system components.

1) *AC/DC Converters*: According to [13], the small-signal dynamics of the VSC can be represented by a three-port AC/DC admittance model as in (1), by which the converters' ac- and dc- side dynamics can be modelled simultaneously.

$$\begin{bmatrix} \Delta \boldsymbol{i}_{\mathrm{g}dq} \\ \Delta i_{\mathrm{dc}} \end{bmatrix} = \begin{bmatrix} \boldsymbol{Y}_{dq} & \boldsymbol{a}_{2\times 1} \\ \boldsymbol{b}_{1\times 2} & Y_{\mathrm{dc}} \end{bmatrix} \cdot \begin{bmatrix} \Delta \boldsymbol{u}_{\mathrm{g}dq} \\ \Delta u_{\mathrm{dc}} \end{bmatrix} \tag{1}$$

where $\Delta \boldsymbol{i}_{\mathrm{g}dq}$ and $\Delta \boldsymbol{u}_{\mathrm{g}dq}$ denote the ac-side dq current and dq voltage, respectively; Δi_{dc} and Δu_{dc} are the dc-side current and voltage, respectively.

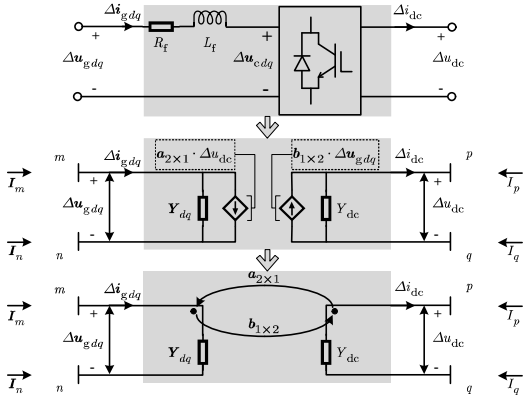

Fig. 1. Equivalent circuit of the three-port admittance model.

Similar to the mutually coupled passive branch [14], the equivalent circuit of such three-port admittance model can be obtained as in Fig. 1, where branch voltage $\Delta \boldsymbol{u}_{\mathrm{g}dq}$, Δu_{dc} can be represented by node voltage $\boldsymbol{V}_m$, $\boldsymbol{V}_n$, V_p, V_q as:

$$\begin{bmatrix} \Delta \boldsymbol{u}_{\mathrm{g}dq} \\ \Delta u_{\mathrm{dc}} \end{bmatrix} = \begin{bmatrix} \boldsymbol{V}_m - \boldsymbol{V}_n \\ V_p - V_q \end{bmatrix} = \underbrace{\begin{matrix} m & n & p & q \end{matrix}}_{} \underbrace{\begin{bmatrix} \boldsymbol{I} & -\boldsymbol{I} & & \\ & & 1 & -1 \end{bmatrix}}_{\boldsymbol{A}} \cdot \begin{bmatrix} \boldsymbol{V}_m \\ \boldsymbol{V}_n \\ V_p \\ V_q \end{bmatrix} \tag{2}$$

where $\boldsymbol{I}$ denotes the second-order identity matrix.

In the same way, branch current $\Delta \boldsymbol{i}_{\mathrm{g}dq}$, Δi_{dc} can be represented by node current $\boldsymbol{I}_m$, $\boldsymbol{I}_n$, I_p, I_q as:

$$\begin{bmatrix} \boldsymbol{I}_m \\ \boldsymbol{I}_n \\ I_p \\ I_q \end{bmatrix} = \underbrace{\begin{matrix} m \\ n \\ p \\ q \end{matrix} \begin{bmatrix} \boldsymbol{I} & \\ -\boldsymbol{I} & \\ & 1 \\ & -1 \end{bmatrix}}_{\boldsymbol{A}^T} \begin{bmatrix} \Delta \boldsymbol{i}_{\mathrm{g}dq} \\ \Delta i_{\mathrm{dc}} \end{bmatrix} \tag{3}$$

By integrating (2) and (3) into (1), the relationship between node voltage and current can be established as:

$$\begin{bmatrix} \boldsymbol{I}_m \\ \boldsymbol{I}_n \\ I_p \\ I_q \end{bmatrix} = \boldsymbol{A}^T \begin{bmatrix} \boldsymbol{Y}_{dq} & \boldsymbol{a} \\ \boldsymbol{b} & Y_{\mathrm{dc}} \end{bmatrix} \boldsymbol{A} \cdot \begin{bmatrix} \boldsymbol{V}_m \\ \boldsymbol{V}_n \\ V_p \\ V_q \end{bmatrix} \tag{4}$$

which can be expanded in matrix form as:

$$\boldsymbol{Y}_{\mathrm{node}}^{con} = \begin{bmatrix} \begin{matrix} & \boldsymbol{m} & \boldsymbol{n} \end{matrix} & & \begin{matrix} & p & q \end{matrix} & \\ \begin{matrix} \boldsymbol{m} \\ \boldsymbol{n} \end{matrix} \begin{bmatrix} \boldsymbol{I} & -\boldsymbol{I} \\ -\boldsymbol{I} & \boldsymbol{I} \end{bmatrix} \begin{bmatrix} \boldsymbol{Y}_{dq} & \\ & \boldsymbol{Y}_{dq} \end{bmatrix} & \begin{matrix} \boldsymbol{m} \\ \boldsymbol{n} \end{matrix} \begin{bmatrix} \boldsymbol{I} & -\boldsymbol{I} \\ -\boldsymbol{I} & \boldsymbol{I} \end{bmatrix} \begin{bmatrix} \boldsymbol{a} & \\ & \boldsymbol{a} \end{bmatrix} \\ \begin{matrix} & \boldsymbol{m} & \boldsymbol{n} \end{matrix} & & \begin{matrix} & p & q \end{matrix} & \\ \begin{bmatrix} \boldsymbol{b} & \\ & \boldsymbol{b} \end{bmatrix} \begin{bmatrix} \boldsymbol{I} & -\boldsymbol{I} \\ -\boldsymbol{I} & \boldsymbol{I} \end{bmatrix} \begin{matrix} p \\ q \end{matrix} & \begin{matrix} p \\ q \end{matrix} \begin{bmatrix} 1 & -1 \\ -1 & 1 \end{bmatrix} Y_{\mathrm{dc}} \end{bmatrix} \tag{5}$$

where building block $\begin{bmatrix} \boldsymbol{I} & -\boldsymbol{I} \\ -\boldsymbol{I} & \boldsymbol{I} \end{bmatrix}$ is used for the node-branch extension of ac-side elements, and building block $\begin{bmatrix} 1 & -1 \\ -1 & 1 \end{bmatrix}$ is used for the node-branch extension of dc elements.

When ac or dc -side of the converter is connected to ground, (5) can be simplified by setting the reference node. For example, if node n is connected to ground, the boundary condition will be $\boldsymbol{V}_n = \boldsymbol{0}, \boldsymbol{I}_n = -\boldsymbol{I}_m$, and the (5) can be simplified as:

$$\boldsymbol{Y}_{\mathrm{node}}^{con} = \begin{bmatrix} \boldsymbol{Y}_{dq} & \boldsymbol{a} & -\boldsymbol{a} \\ \boldsymbol{b} & Y_{\mathrm{dc}} & -Y_{\mathrm{dc}} \\ -\boldsymbol{b} & -Y_{\mathrm{dc}} & Y_{\mathrm{dc}} \end{bmatrix} \tag{6}$$

In particular, if both ac and dc side are connected to ground, the boundary condition will be $\boldsymbol{V}_n = \boldsymbol{0}, \boldsymbol{I}_n = -\boldsymbol{I}_m, V_q = 0, I_q = -I_p$, and (5) will degenerate to (1).

2) *AC Passive Components*: Supposing the admittance of the ac branch $\boldsymbol{kl}$ is $\boldsymbol{Y}_{dq}^{kl}$, the corresponding building block can be constructed as:

$$\boldsymbol{Y}_{\mathrm{node}}^{ac} = \begin{matrix} & \boldsymbol{k} & \boldsymbol{l} \end{matrix} \begin{matrix} \boldsymbol{k} \\ \boldsymbol{l} \end{matrix} \begin{bmatrix} \boldsymbol{I} & -\boldsymbol{I} \\ -\boldsymbol{I} & \boldsymbol{I} \end{bmatrix} \cdot \begin{bmatrix} \boldsymbol{Y}_{dq}^{kl} & \\ & \boldsymbol{Y}_{dq}^{kl} \end{bmatrix} \tag{7}$$

3) *DC Passive Components*: Supposing the admittance of the dc branch *eh* is Y_{dc}^{eh}, the corresponding building block can be constructed as:

$$Y_{\mathrm{dc}}^{dc} = \begin{matrix} & e & h \end{matrix} \begin{matrix} e \\ h \end{matrix} \begin{bmatrix} 1 & -1 \\ -1 & 1 \end{bmatrix} \cdot Y_{\mathrm{dc}}^{eh} \tag{8}$$

B. System Network Modelling

By rotating the converter's impedance model evaluated in respective *dq*-local reference frame to the same *dq*-global reference frame [15], the system network matrix can be constructed in a systematic building-block manner. According to (5), (7) and (8), the node-branch incidence matrix $\boldsymbol{A}$ for the hybrid AC/DC grid is defined in (9). To avoid the singularity, at least one reference node needs to be selected for each AC or DC subsystem.

$$a_{ij} = \begin{cases} \boldsymbol{0} \,/\, 0 & \mathrm{branch}_i \text{ not connected to node}_j \\ \boldsymbol{I} \,/\, 1 & \mathrm{branch}_i \text{ current outflow node}_j \\ -\boldsymbol{I} \,/\, -1 & \mathrm{branch}_i \text{ current inflow node}_j \end{cases} \tag{9}$$

The node admittance matrix $\boldsymbol{Y}_{\mathrm{node}}(s)$ can be obtained:

$$\boldsymbol{Y}_{\mathrm{node}}(s) = \boldsymbol{A}^T \cdot \boldsymbol{Y}_{\mathrm{br}}(s) \cdot \boldsymbol{A} \tag{10}$$

where $\boldsymbol{Y}_{\mathrm{br}}(s)$ represents the branch admittance matrix.

The system stability can be determined by calculating the RHP-zero of $\boldsymbol{Y}_{\mathrm{node}}(s)$ as in (11). The system is stable if and only if there exists no RHP-zero.

$$\det\left[\boldsymbol{Y}_{\mathrm{node}}(s)\right] = 0 \Rightarrow \text{RHP-zero} \tag{11}$$

C. Modification of Network Model

The above building-block approach can also provide insight for developing algorithms to account for network changes. By superposing the modification matrix on the original network matrix (add or subtract), the new system network model can be obtained conveniently. Considering a n-node system, modification matrices for AC/DC converters and AC/DC passive components are given:

The modification matrix for converter j (e.g., dc-side connected to ground) is like:

$$\Delta \boldsymbol{Y}_{\text{node}} = \begin{array}{c} \\ \boldsymbol{m} \\ \\ \boldsymbol{n} \\ \\ p \\ \\ \end{array} \begin{array}{c} \begin{array}{ccccccc} \boldsymbol{m} & & \boldsymbol{n} & & p & & \end{array} \\ \begin{bmatrix} \cdot & \cdot & \cdot & \cdot & \cdot & \cdot & \cdot \\ \cdot & \boldsymbol{Y}_{dq}^{j} & \cdot & -\boldsymbol{Y}_{dq}^{j} & \cdot & -\boldsymbol{a}^{j} & \cdot \\ \cdot & \cdot & \cdot & \cdot & \cdot & \cdot & \cdot \\ \cdot & -\boldsymbol{Y}_{dq}^{j} & \cdot & \boldsymbol{Y}_{dq}^{j} & \cdot & \boldsymbol{a}^{j} & \cdot \\ \cdot & \cdot & \cdot & \cdot & \cdot & \cdot & \cdot \\ \cdot & -\boldsymbol{b}^{j} & \cdot & \boldsymbol{b}^{j} & \cdot & Y_{\text{dc}}^{j} & \cdot \\ \cdot & \cdot & \cdot & \cdot & \cdot & \cdot & \cdot \end{bmatrix}_{n\times n} \end{array} \tag{12}$$

The modification matrix for AC passive components (e.g., $\boldsymbol{Y}_{dq}^{kl}$) is like:

$$\Delta \boldsymbol{Y}_{\text{node}} = \begin{array}{c} \\ \boldsymbol{k} \\ \\ \boldsymbol{l} \\ \\ \end{array} \begin{array}{c} \begin{array}{ccccc} & \boldsymbol{k} & & \boldsymbol{l} & \end{array} \\ \begin{bmatrix} \cdot & \cdot & \cdot & \cdot & \cdot \\ \cdot & \boldsymbol{Y}_{dq}^{kl} & \cdot & -\boldsymbol{Y}_{dq}^{kl} & \cdot \\ \cdot & \cdot & \cdot & \cdot & \cdot \\ \cdot & -\boldsymbol{Y}_{dq}^{kl} & \cdot & \boldsymbol{Y}_{dq}^{kl} & \cdot \\ \cdot & \cdot & \cdot & \cdot & \cdot \end{bmatrix}_{n\times n} \end{array} \tag{13}$$

The modification matrix for DC passive components (e.g., Y_{dc}^{eh}) is like:

$$\Delta \boldsymbol{Y}_{\text{node}} = \begin{array}{c} \\ e \\ \\ h \\ \\ \end{array} \begin{array}{c} \begin{array}{ccccc} & e & & h & \end{array} \\ \begin{bmatrix} \cdot & \cdot & \cdot & \cdot & \cdot \\ \cdot & Y_{\text{dc}}^{eh} & \cdot & -Y_{\text{dc}}^{eh} & \cdot \\ \cdot & \cdot & \cdot & \cdot & \cdot \\ \cdot & -Y_{\text{dc}}^{eh} & \cdot & Y_{\text{dc}}^{eh} & \cdot \\ \cdot & \cdot & \cdot & \cdot & \cdot \end{bmatrix}_{n\times n} \end{array} \tag{14}$$

III. FMA-BASED OSCILLATION ANALYSIS

In this section, a typical hybrid AC/DC grid shown in Fig. 1 is selected as the test system, whose parameters can be referred to [16], [17].. Three wind farms (WFs) are interconnected with the AC grid via a four-terminal HVDC transmission system, containing two sending converter (SEC) stations and two receiving converter (REC) stations.

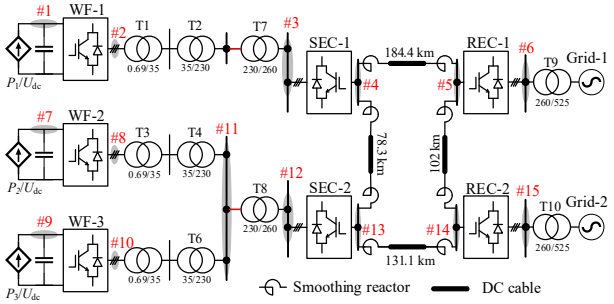

Fig. 2. A typical hybrid AC/DC grid.

The directed graph of the studied system is presented in Fig. 3, where the relationships among nodes (vertices) and branches (edges) are represented in topologic graph way.

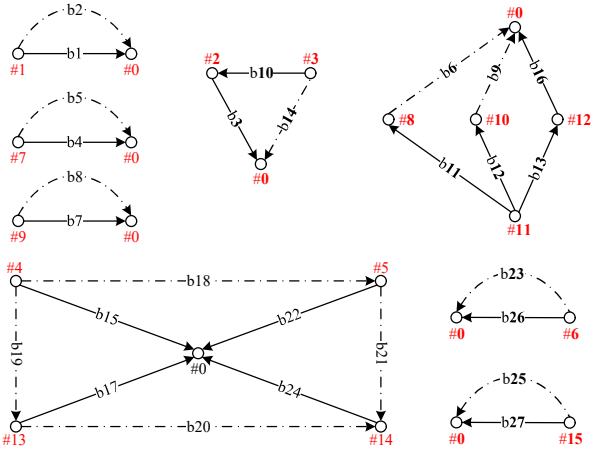

Fig. 3. Directed graph of the studied system.

According to Fig. 3, the node-branch incidence matrix $\boldsymbol{A}$ can be established using (9). By integrating $\boldsymbol{A}$ and system branch admittance matrix into (10), the node admittance matrix can be obtained, whose concrete expression is given in [16].

A. Stability Judgement

By increasing the internal inductance of the Grid-1 in Fig. 2 from 4mH to 8mH, an oscillation will be induced in the system. With the substitution of this marginal condition (i.e., 8mH) into the node admittance matrix $\boldsymbol{Y}_{\text{node}}(s)$, the pole-zero distribution can be calculated as shown in Fig. 4. It can be observed that there exists one pair of RHP-zeros, denoting that the system is unstable and the frequency of the oscillation mode is 7.9Hz (49.9rad/s) in *d-q* frame.

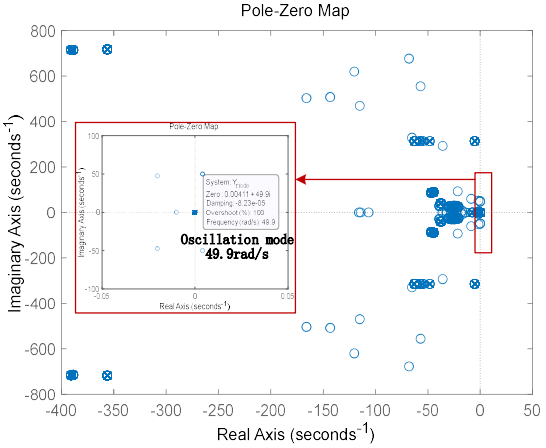

Fig. 4. Pole-zero distribution.

The FFT analysis results and the corresponding time-domain simulation results are given in Fig. 4 and Fig. 5, respectively. It can be observed that the system will become unstable when the internal inductance of the grid-1 is increased from 4mH to 8mH. The oscillation frequency is 42Hz and 58Hz in stationary frame (i.e., 8Hz in *d-q* frame). Therefore, the simulation results are consistent with the above theoretical analysis results, which also validates the accuracy of the proposed frequency-domain network modelling method.

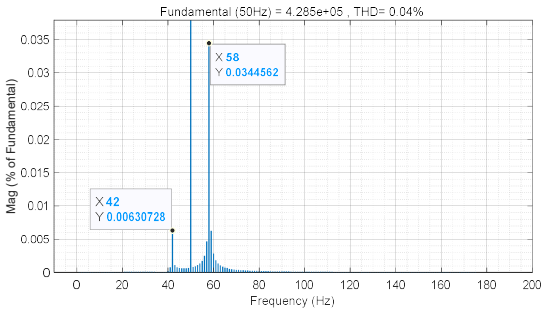

Fig. 5. FFT analysis results.

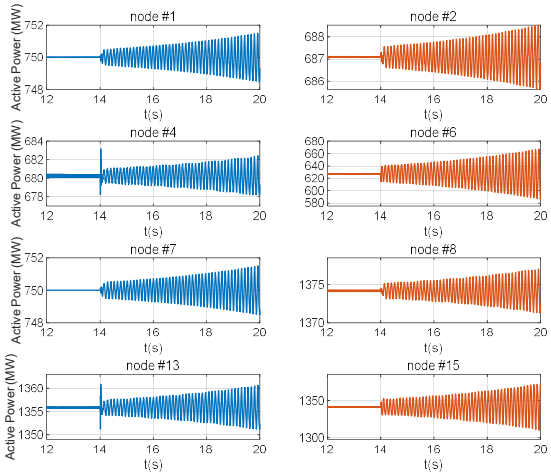

Fig. 6. FFT analysis results.

B. Oscillation Diagnosis

Suppose an oscillation at frequency f occurs (typically corresponds to the RHP-zeros of the system), the node admittance matrix $[\boldsymbol{Y}(s_m)]$ will approach singularity, which can be decomposed as:

$$\boldsymbol{Y}(s_m) = \boldsymbol{R}\boldsymbol{\Lambda}\boldsymbol{L} \tag{15}$$

where $\boldsymbol{\Lambda}=\mathrm{diag}(\lambda_1,\lambda_2,\ldots\lambda_n)$ represents the diagonal eigenvalue matrix, $\boldsymbol{R}=[\boldsymbol{r}_1,\boldsymbol{r}_2,\ldots,\boldsymbol{r}_n]$ denotes the right eigenvector, and $\boldsymbol{L}=[\boldsymbol{l}_1^{\mathrm{T}},\boldsymbol{l}_2^{\mathrm{T}},\ldots,\boldsymbol{l}_n^{\mathrm{T}}]^{\mathrm{T}}$ is the left eigenvector.

The controllability (Con) and observability (Obs) of the oscillation mode are characterized by $[\boldsymbol{R}]$ and $[\boldsymbol{L}]$ respectively, which can be combined into a single index——participation factor (PF). The node Con, Obs and PF are defined as:

$$\begin{aligned} Obs_{\mathrm{node}} &= [\boldsymbol{r}_m]_{\mathrm{node}},\ Con_{\mathrm{node}} = [\boldsymbol{l}_m]_{\mathrm{node}} \\ PF_{\mathrm{node}} &= \mathrm{diag}\left([\boldsymbol{r}_m]_{\mathrm{node}} \cdot [\boldsymbol{l}_m]_{\mathrm{node}}\right) \end{aligned} \tag{16}$$

With the node oscillation information, the branch oscillation information can be obtained as:

$$\begin{aligned} Obs_{\mathrm{branch}} &= \boldsymbol{A}[\boldsymbol{r}_m]_{\mathrm{node}},\ Con_{\mathrm{branch}} = [\boldsymbol{l}_m]_{\mathrm{node}}\boldsymbol{A}^{\mathrm{T}} \\ PF_{\mathrm{branch}} &= \mathrm{diag}\left(\boldsymbol{A}[\boldsymbol{r}_m]_{\mathrm{node}}[\boldsymbol{l}_m]_{\mathrm{loop}}\boldsymbol{A}^{\mathrm{T}}\right) \end{aligned} \tag{17}$$

Based on the identified oscillation mode shown in Fig. 4, the node and branch oscillation information including Obs, Con and PF are calculated in Table I and Table II, respectively. From Table I, dominant nodes include #4, #6, #13 and #14 with high PF. From Table II, dominant branches contain b23, b25, b26 and b27 with high PF. Therefore, the FMA analysis indicates that the oscillation source should be located at node #6 and branch b23, b26. This is consistent with the time-domain simulation that the oscillation is stimulated from the inductance of the grid-1 (located in node #6, branch b26).

TABLE I
FMA ANALYSIS RESULTS (NODE)

node	PF (p.u.)	Obs (p.u.)	Con (p.u.)
#1	4.48e-07	2.24e-04	2.21e-04
#2	0.0078	0.0186	0.0463
#3	0.014	0.0191	0.0663
#4	**0.1427**	0.1579	0.1002
#5	0.0913	0.1263	0.0802
#6	**0.3247**	0.1931	0.1865
#7	5.49e-07	2.45e-04	2.48e-04
#8	0.0095	0.0201	0.0523
#9	5.49e-07	2.45e-04	2.48e-04
#10	0.0095	0.0201	0.0523
#11	0.0125	0.0202	0.0687
#12	0.0138	0.0207	0.0736
#13	**0.1641**	0.1693	0.1075
#14	**0.1893**	0.1818	0.1154
#15	0.0234	0.0521	0.0499

TABLE II
FMA ANALYSIS RESULTS (BRANCH)

branch	PF (p.u.)	Obs (p.u.)	Con (p.u.)
b1	1.12e-10	3.69e-06	3.96e-06
b2	1.12e-10	3.69e-06	3.96e-06
b3	8.58e-05	0.0023	0.0049
b4	1.22e-10	3.81e-06	4.15e-06
b5	1.22e-10	3.81e-06	4.15e-06
b6	1.21e-04	0.0025	0.0061
b7	1.22e-10	0.0023	4.15e-06
b8	1.22e-10	0.0025	4.15e-06
b9	1.21e-04	0.0025	0.0061
b10	8.58e-05	0.0051	0.0049
b11	1.21e-04	0.0023	0.0061
b12	1.21e-04	0.0037	0.0061
b13	4.81e-04	0.0051	0.0123
b14	8.58e-05	0.0023	0.0049
b15	7.51e-05	0.0037	0.0026
b16	4.81e-04	0.0051	0.0123
b17	2.52e-04	0.0068	0.0048
b18	0.0032	0.0241	0.0170
b19	0.0024	0.0209	0.0147
b20	0.0016	0.0172	0.0121
b21	0.0363	0.0817	0.0577
b22	0.0607	0.1057	0.0746
b23	**0.2922**	0.1840	0.2062
b24	0.0527	0.0984	0.0695
b25	**0.1284**	0.1232	0.1353
b26	**0.2922**	0.1840	0.2062
b27	**0.1284**	0.1232	0.1353

IV. MAPPING RELATIONSHIP BETWEEN FMA RESULTS AND MEASUREMENT DATA

As stated above, it is more preferred that oscillation information obtained from the FMA can also be extracted from the measurement data, e.g., real-time voltage/current, so as to realize the data-driven oscillation diagnosis. Actually, the FMA results can be acquired via the active measurement method [12], i.e., performing N times

voltage or current injections at mode frequency for all N nodes or loops. However, the application of such method is cumbersome (N times injections) and the active injection adopted may affect the system operation. In practice, the real-time voltage and current are the most accessible data. By performing some data processing (e.g., FFT analysis), the oscillation frequency f_{mea} and the divergence degree $D_{\text{mea}}(t)$ at each node/branch can be extracted. The divergence degrees of node voltage and branch current are defined in (18):

$$\begin{aligned} D^{v}_{\text{node}}(t) &= \left(v_{\text{node}}(t) - U_{\text{node}}\right)/U_{\text{node}} \\ D^{i}_{\text{branch}}(t) &= \left(i_{\text{branch}}(t) - I_{\text{branch}}\right)/I_{\text{branch}} \end{aligned} \tag{18}$$

where $v_{\text{node}}(t)$ and $i_{\text{branch}}(t)$ denote the real-time node voltage and branch current, respectively. U_{node} and I_{branch} are the steady-state value under the stable operation.

Generally speaking, the measured divergence degree has no rigorous mathematical relationship with the FMA-derived Obs, Con and PF [11]. However, from the practical experience, the nodes/branches with large divergence degree are usually those with high Obs and PF, implying the location information of the possible oscillation source. This is validated in Table III, where the measurement results of Obs are basically consistent with the FMA results (voltage data taken at 18s shown in Fig. 6). Besides, the node with highest Obs, i.e., #6, is the location of the oscillation source. Therefore, with the measurement data, the oscillation source can be roughly determined.

TABLE III
COMPARISON BETWEEN FMA RESULTS AND MEASUREMENTS DATA

node	Obs (FMA)	Obs (Measurement)	error (%)
#1	2.2437×10^{-5}	2.1314×10^{-5}（0.0897V）	-5.01
#2	1.8607×10^{-2}	1.8783×10^{-2}（79.048V）	0.95
#3	1.9123×10^{-2}	1.9304×10^{-2}（81.241V）	0.95
#4	$\mathbf{1.5788\times10^{-1}}$	$\mathbf{1.5639\times10^{-1}}$（658.15V）	-0.94
#5	1.2629×10^{-1}	1.2292×10^{-1}（517.32V）	-2.67
#6	$\mathbf{1.9306\times10^{-1}}$	$\mathbf{2.0339\times10^{-1}}$（855.99V）	5.35
#7	2.4544×10^{-5}	2.6232×10^{-5}（0.1104V）	6.88
#8	2.0088×10^{-2}	2.0278×10^{-2}（85.339V）	0.94
#9	2.4544×10^{-5}	2.6232×10^{-5}（0.1104V）	6.88
#10	2.0088×10^{-2}	2.0278×10^{-2}（85.339V）	0.94
#11	2.0214×10^{-2}	2.0405×10^{-2}（85.875V）	0.92
#12	2.0728×10^{-2}	2.0924×10^{-2}（88.059V）	0.95
#13	$\mathbf{1.6929\times10^{-1}}$	$\mathbf{1.6667\times10^{-1}}$（701.44V）	-1.55
#14	$\mathbf{1.8182\times10^{-1}}$	$\mathbf{1.7801\times10^{-1}}$（749.15V）	-2.10
#15	5.2081×10^{-2}	5.2574×10^{-2}（221.26V）	0.89

Enlighted by such qualitative knowledge, the mapping relationship between the FMA results and the measurement data can be identified through large numbers of case match trainings. As shown in Fig. 7, by simulating various oscillation cases, multiple sets of FMA results and measurement divergence degree can be obtained, the mapping relationship between which can be identified and optimized. With such mapping relationship, the oscillation source information can be directly extracted from the measurement data rather than the complicated theoretical model-based analysis.

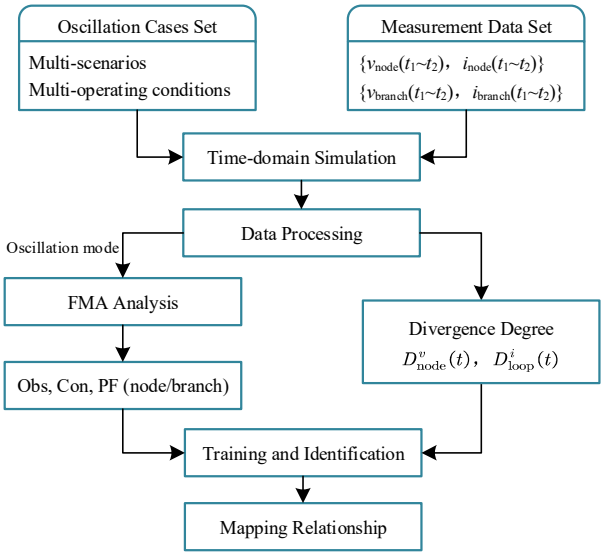

Fig. 7. Mapping relationship acquisition procedure.

V. CONCLUSION

In this paper, the frequency-domain network model of the power electronics-dominated hybrid AC/DC grid is established and validated. Based on such model, the FMA-based oscillation analysis is carried out and the oscillation source can be identified via the participation factor results, including the Obs, Con and PF. At last, the procedure of acquiring the mapping relationship between the FMA results and the measurement data is given, laying the ground of the future data-driven oscillation diagnosis.

ACKNOWLEDGMENT

The authors would like to acknowledge the open access publication support to the project “NTNU-Chinese Collaboration on Next Generation Power Electronics Converters for Renewable Energy (CoNeCt)” 309253 funded by the Research Council of Norway under the INTPART programme. This work was also supported in part by the National Natural Science Foundation of China under Grant 51837007.

REFERENCES

[1] B. Mohandes, M. S. E. Moursi, N. Hatziargyriou and S. E. Khatib, "A Review of Power System Flexibility With High Penetration of Renewables," *IEEE Trans. Power Syst.*, vol. 34, no. 4, pp. 3140-3155, July 2019.

[2] A. Khan, M. Hosseinzadehtaher, M. B. Shadmand, S. Bayhan and H. Abu-Rub, "On the Stability of the Power Electronics-Dominated Grid: A New Energy Paradigm," *IEEE Trans. Ind. Electron. Mag.*, vol. 14, no. 4, pp. 65-78, Dec. 2020.

[3] C. Liu, F. Deng, Q. Heng, X. Cai, R. Zhu and M. Liserre, "Crossing Thyristor Branches-Based Hybrid Modular Multilevel Converters for DC Line Faults," *IEEE Trans. Ind. Electron.*, vol. 68, no. 10, pp. 9719-9730, Oct. 2021.

[4] J. Lyu, X. Cai and M. Molinas, "Frequency Domain Stability Analysis of MMC-Based HVdc for Wind Farm Integration," *IEEE J. Emerg. Sel. Topics Power Electron.*, vol. 4, no. 1, pp. 141-151, March 2016.

[5] H. Zong, J. Lyu, X. Wang, C. Zhang, R. Zhang, and X. Cai, "Grey box aggregation modeling of wind farm for wideband oscillations analysis," *Apply Energy*, vol. 283, no. 1, pp. 116035, 2021.
[6] C. Zhang, X. Cai, A. Rygg and M. Molinas, "Sequence Domain SISO Equivalent Models of a Grid-Tied Voltage Source Converter System for Small-Signal Stability Analysis," *IEEE Trans. Energy Convers.*, vol. 33, no. 2, pp. 741-749, June 2018.
[7] H. Zong, C. Zhang, J. Lyu, X. Cai and M. Molinas, "Block Diagonal Dominance-Based Model Reduction Method Applied to MMC Asymmetric Stability Analysis," *IEEE Trans. Energy Convers.*, vol. 36, no. 3, pp. 2438-2451, Sept. 2021.
[8] J. Sun, "Impedance-Based Stability Criterion for Grid-Connected Inverters," *IEEE Trans. Power Electron.*, vol. 26, no. 11, pp. 3075-3078, Nov. 2011.
[9] J. Cao, W. Du, H. Wang, Z. Chen and H. F. Li, "A Novel Emergency Damping Control to Suppress Power System Inter-Area Oscillations," *IEEE Trans. Power Syst.*, vol. 28, no. 3, pp. 3165-3173, Aug. 2013.
[10] Y. Wang, X. Jiang, X. Xie, X. Yang and X. Xiao, "Identifying Sources of Subsynchronous Resonance Using Wide-Area Phasor Measurements," *IEEE Trans. Power Del.*, vol. 36, no. 5, pp. 3242-3254, Oct. 2021.
[11] Wilsun Xu, Zhenyu Huang, Yu Cui and Haizhen Wang, "Harmonic resonance mode analysis," *IEEE Trans. Power Del.*, vol. 20, no. 2, pp. 1182-1190, April 2005.
[12] Y. Zhan, X. Xie, H. Liu, H. Liu and Y. Li, "Frequency-Domain Modal Analysis of the Oscillatory Stability of Power Systems With High-Penetration Renewables," *IEEE Trans. Sustain. Energy*, vol. 10, no. 3, pp. 1534-1543, July 2019
[13] J. Pedra, L. Sainz and L. Monjo, "Three-Port Small Signal Admittance-Based Model of VSCs for Studies of Multi-Terminal HVDC Hybrid AC/DC Transmission Grids," *IEEE Trans. Power Syst.*, vol. 36, no. 1, pp. 732-743, Jan. 2021.
[14] J. J.Grainger and J. William D. Stevenson, *Power system analysis*. 1994. McGraw-Hill, Inc.
[15] H. Zong, J. Lyu, X. Cai, C. Zhang, M. Molinas, and F. Rao, "Accurate aggregated modelling of wind farm systems in modified sequence domain for stability analysis," *Electric Power Syst. Res*., vol. 175, Oct. 2019, Art. no. 105928.
[16] H. Zong, C. Zhang, X. Cai and M. Molinas, "Oscillation Propagation Analysis of Hybrid AC/DC Grids with High Penetration Renewables," *IEEE Trans. Power Syst.*, to be published.
[17] R. Yang, G. Shi, X. Cai, C. Zhang, G. Li and J. Liang, "Autonomous Synchronizing and Frequency Response Control of Multi-terminal DC Systems With Wind Farm Integration," *IEEE Trans. Sustain. Energy*, vol. 11, no. 4, pp. 2504-2514, Oct. 2020.